Geomechanics and Engineering, *Vol. 39, No. 6 (2024) 611-627*
https://doi.org/10.12989/gae.2024.39.6.611

Deformation of geogrid-reinforced soil wall: Usage of random forests regression analysis

Jiaman Li[1a] and Xing Gao*[2]

[1]*School of Architecture and Surveying Engineering, Shaanxi College of Communication Technology, Xi'an 710018, Shaanxi, China*
[2]*Capital Construction Department, Yantai Yuhuangding Hospital, Yantai 264000, Shandong, China*

(*Received May 24, 2024, Revised December 16, 2024, Accepted December 18, 2024*)

Abstract. An essential component of designing geosynthetic reinforced soil walls ($GRSW$) is deformation analysis. Nonetheless, research highlights how artificial intelligence techniques may be used to solve geotechnical engineering problems. This study's primary goal was to investigate the potential use of machine learning-based techniques for $GRSW$ deformation (Dis) estimate. This paper presents and validates new methods that combine random forests (RF) with the ant lion optimization ($AnOA$), the chimp optimization algorithm ($ChOA$), and the gannet optimization algorithm ($GaOA$). The dataset for this purpose was created by combining 166 finite element studies that have been done in the literature. The findings presented that the $RF(AnOA)$, $RF(ChOA)$, and $RF(GaOA)$ methods have a significant ability to accurately predict the Dis of $GSRW$ with R^2 values larger than 0.976. The value of Theil inequality coefficient (TIC) was 0.0463 and 0.0282 in the learning and examining sections for $RF(GaOA)$, remarkably smaller than those of $RF(ChOA)$ at 0.0523 and 0.063, and $RF(AnOA)$ by 0.0564 and 0.0799, respectively. In conclusion, the results suggest that the suggested models may be used to evaluate the effectiveness of geosynthetic reinforced soil structures. This research provides a significant contribution by establishing a scalable and efficient framework for evaluating the deformation performance of $GRSW$ structures, bridging the gap between computational geomechanics and machine learning. The proposed RF models can replace or complement traditional numerical methods for estimating $GRSW$ deformation, saving time and computational resources. Using these models, engineers can predict $GRSW$ deformations with high precision, enabling more accurate design and better safety assessments of geotechnical structures.

Keywords: displacement; estimation; geogrid; GRS wall; hyperparameter; random forests; sensitivity analysis

1. Introduction

Geotechnical engineering has seen a significant focus on the examination and application of geosynthetic-reinforced soil walls ($GRSW$) in recent times (Afkhami hoor and Esmaeili-Falak 2025). These walls are notable for their numerous benefits over gravity retaining walls. A beautiful structure, proper distortion, economic efficiency, and faster construction are the benefits (Leshchinsky and Han 2004, Yang *et al*. 2016, Hassankhani and Esmaeili-Falak 2024).

Building earth-retaining buildings in mountainous areas with high elevation and steepness has become common due to infrastructural growth. These designs are efficient, according to many empirical instances. As the vertical dimension of the wall grows, the necessary tensile strength for a single $GRSW$ frequently increases significantly (Leshchinsky *et al.* 2004, Liu 2012). The suggested technique strategically reduces the vertical distance between $GRSW$ to improve reinforcement tensile strength. However, this technology requires more geosynthetic layers, increasing costs. High $GRSW$ in a tiered design is a popular way to reduce reinforcing tensile stress. This method works well in circumstances when there is adequate space available (Elias *et al*. 2001, Stuedlein *et al.* 2010, Yoo and Jung 2004, Yoo and Kim 2008).

By intelligently placing reinforcements and employing high-tensile materials, $GRSW$s assure internal, external, and global stability. Scholars suggest many analytical methods for $GRSW$ development (Allen *et al*. 2002, Berg *et al*. 2009, Lemonnier *et al.* 1998, Mandal and Jambale 1992). Design criteria often employ limit equilibrium and lateral earth pressure to define $GRSW$ reinforcing elements that reduce failure risk (Carter and Bernardi 2014, Officials 2009). However, the limited balancing technique cannot accurately predict deformations and ignores the relationship between backfill material stress and strain and $GRSW$ system component interactions. Instead, the result depends on assumptions regarding failure and crucial slip plane identification (Mo *et al.* 2007). In recent years, quantitative methods for $GRSW$ stability and deformation analysis have developed. Numerous scholars have used parametric computational methods to analyze how design factors affect $GRSW$ lateral deformations (Bathurst *et al*. 2010, Rowe and Ho 1998, Wu and Pham 2010). The maximum lateral displacement throughout construction is used to evaluate $GRSW$. This component is crucial to $GRSW$ effectiveness evaluation.

The maximum horizontal displacement of $GRSW$ in the US was 3.5% of wall height (H) (Carter and Bernardi 2014). Many empirical methods have been tested to predict

*Corresponding author, Researcher
E-mail: 13465587619@163.com
[a]M.Sc

ISSN: 2005-307X (Print), 2092-6219 (Online)

the horizontal displacement of a GRSW on a rigid basis (Wu and Pham 2010). The preceding approaches do not account for stiffness and reinforcing creep on face horizontal deflections. Thus, realistic horizontal displacement prediction is dubious (Kazimierowicz-Frankowska 2018, Khosrojerdi *et al*. 2017, 2020). $GRSW$s are increasingly used to help disperse bases on bridge abutments instead of deep bases. Numerous inquiries and computer simulations have examined the horizontal displacements and load-bearing capabilities of $GRSW$ with a flexible face under dispersed footing loads (Adams *et al.* 2012, Epstein *et al*. 2018, Wu *et al*. 2006, Yaychi and Esmaeili-Falak 2024). The empirical technique predicts $GRSW$ greatest horizontal displacement under distributed footing loads regardless of offset interval (Khosrojerdi *et al.* 2020). The greatest lateral motion and factor of safety (FS) acquired using the enhanced Bishop approach have led to a suggested method to forecast the lateral movement of a $GRSW$ with a flexible face (Rahmaninezhad and Han 2021).

In a research investigation, two well-known slope stability methods were compared (Alias *et al.* 2017). The adaptive neuro-fuzzy inference system ($ANFIS$) and artificial neural networks (ANN) are widely used in academia and industry (Armaghani *et al*. 2020, Liu *et al*. 2021, Mirzaeiabdol yousefi *et al*. 2022, Esmaeili-Falak and Sarkhani 2024). Research aimed to anticipate numerous FS values for a long-lasting structure. In accordance with academic research, the $ANFIS$ structure outperforms the ANN technique in all FS classes. Ozturk employed ANN to predict and evaluate retaining wall (RW) seismic movements in a significant study (Ozturk 2014). Under a previous study, ANN and ant colony optimization were utilized to forecast and enhance RW structure fault tolerance under dynamic conditions (Xu *et al.* 2019). In dynamic situations, Chen et al. used two linked ANN-based layouts, the genetic algorithm (GA) and the imperialist competitive algorithm (ICA), to enhance RW FS estimates (Chen *et al*. 2019). $ICA-ANN$ was less effective than $GA-ANN$. A report tested two soft computing methods for $GRSW$ deformation prediction. So, 166 finite element studies were done to build the data set. Next, two $GRSW$ displacement forecasting algorithms were created. To develop an intelligent model, two ANN were combined with the Gravitational Search Algorithm (GSA) and Particle Swarm Optimization (PSO), respectively. GSA- and PSO-based ANN prediction models function well. The correlation coefficient (R) of 0.981 for testing data suggests that the GSA-based ANN prediction version surpasses the PSO-based version with R of 0.973 (Momeni *et al*. 2021).

To forecast GRS abutment settling, ANN and Harris hawks' optimization (HHO) were used to create an integrated AI system. The results showed that the $ANN-HHO$ system estimated GRS abutment settling accurately and outperformed other models. Thus, geotechnical/civil engineers use it to anticipate GRS abutment in-service performance before making a choice (Raja *et al.* 2022). A novel hybrid method for forecasting GRS foundation ($GRSF$) settlement uses evolutionary algorithm grey-wolf optimisation (GWO) and ANN. Numerical simulations on verified large-scale 3-D finite element models provided dependable relevant data. Findings show that the combined $ANN-GWO$ system can reliably and intelligently assess $GRSF$ ultimate settlement under service loads, making it a predictive tool for $GRSF$ preliminary design (Raja and Shukla 2021). According to the above discussion, soft computing approaches effectively handle mechanical stabilized earth and reinforced wall system issues. However, further research employing more extensive and accurate methods is needed to explore these challenges.

In accordance with the framework of this research on Random Forests (RF) using optimization techniques, it is worth examining the effective use of this software for estimate in many disciplines (Islam *et al.* 2022, Joo *et al.* 2022, Probst *et al.* 2019). The objective of integrating optimizer algorithms with the RF concept is to determine the optimum values of hyperparameters. The assessment of landslide susceptibility mapping is performed by integrating RF with Bayesian hyperparameter optimization (Sun *et al.* 2020, 2021, Wang *et al.* 2021). A novel technique was devised for geographical predictive mapping of mineral prospectivity by optimizing the hyperparameters of the RF model using a genetic algorithm (Mehrdad Daviran *et al.* 2021). Landslide susceptibility is estimated through the use of a genetic optimization approach to tune the hyperparameters of a RF model (Daviran *et al*. 2023). The improved RF framework is used to diagnose Heart Disease, with the random search approach being used for hyperparameter tuning (Javeed *et al.* 2019). The major purpose of a work was to evaluate the potential utilize of machine learning-based approaches in forecasting the deformation of geogrid-reinforced soil structure (Dis). Th study introduced novel techniques that integrate the reptile search algorithm (RSA) and equilibrium optimizer (EO) with least squared support vector regression (LSSVR). The results show that both the LSSVRE and LSSVRR algorithms have a good chance of correctly forecasting the Dis. A comprehensive index named OBJ concluded 1.8003 for LSSVRE, and an almost a half reduction at 0.9257 for LSSVRR (Chien-Ta *et al*. 2024).

1.1 The principal objective

In summary, the important stages and contributions of the present work may be enumerated as follows:

- A vast and verified data is used in the procedure of building and evaluating machine learning algorithms to assess the deformation of $GRSW$. It is important to highlight that a large fraction of earlier research studies have relied mostly on datasets of limited size.
- There are several designs that have been offered, however there aren't many research that specifically look at using random forests (RF) to predict deformation in soil structures reinforced with geogrids.
- The problem of model selection—that is, figuring out appropriate hyper-parameters—is very important. This paper enounced the application of novel techniques that integrated the RF regression analysis with ant lion optimization ($AnOA$), Chimp optimization algorithm

Table 1 Statistical characteristics of the dependent and independent parameters

Stage	Index							
	Minimum	Maximum	Standard Deviation	Average	Kurtosis	Skewness	Median	Range
Independent parameters								
			$q\ (kpa)$					
Training	20	80	21.918	47.419	-1.2977	0.1465	40	60
Testing	20	80	21.925	49.524	-1.3181	0.0606	40	60
			$E\ /\ E_0$					
Training	0.25	4	1.378	1.5806	-0.744	0.8556	1	3.75
Testing	0.25	4	1.3386	1.8512	-1.0175	0.612	2	3.75
			$S_v\ (m)$					
Training	15	60	17.767	33.024	-1.174	0.5958	30	45
Testing	15	60	20.215	36.428	-1.8412	0.181	30	45
			$\varphi\ (°)$					
Training	32	44	4.93	38.29	-1.526	-0.089	38	12
Testing	32	44	4.712	38.286	-1.396	-0.084	38	12
Dependent parameter								
			$Dis\ (mm)$					
Training	1.49	91.27	23.367	25.3	0.9743	1.2657	17.05	89.786
Testing	1.753	84.76	22.87	22.366	1.894	1.6307	13.086	83.009

($ChOA$), and Gannet optimization algorithm ($GaOA$).

• Depicting the displacement of the $GRSW$ using experimental tests or numerical analysis need cost, energy and tools. These shortcomings could be solved roughly employing machine learning-based models.

• The sensitivity analysis was performed in order to depict the impact of each input parameter on the target.

• Finally, the limitations of this study were addressed and some suggestion provided for future studies.

2. Methodology

2.1 Dataset pre-processing

This research examined the surcharge load, friction angle, geosynthetic stiffness, and vertical spacing between geogrid layers as the key elements of investigation in the $GSRW$. The influence of minor parameters such as soil-foundation friction angles and surface modular blocks on the performance of GRS structures is evident, so was not included as one of the input parameters. Obtaining or assembling a substantial sample in the field of geotechnical engineering also presents some difficulties. Therefore, it is not preferable to introduce additional factors; rather, it is advised to remove less relevant aspects. A comprehensive collection of 166 finite element studies was compiled from the research literature, and the resultant values were subsequently employed as simulation variables (Momeni *et al.* 2021). The data set was divided into two distinct stages training and evaluation. 25% (42 examples) of the data set were allocated for the assessment step, and the remaining 75% (124 examples) were designated for the learning process (Dawei *et al*. 2023, Zhang *et al*. 2024).

To make sure that every data point was incorporated in both the training and testing phases, the data collected was divided into two separate subsets. Additionally, the partitioning procedure upheld the norms of a normal distribution. Statistical information about the independent and dependent factors is included in Table 1.

Variables introduced for creating the hybrid RF models consist of:

- Input parameters
  - Surcharge ($q\ (kPa)$)
  - Reinforcement stiffness ratio (E/E_0) (E_0 is the initial large-scale reinforcement stiffness = 11.5 KN/m)
  - friction angle (Φ (°))
  - the vertical space of the geogrid layers is ($S_v\ (m)$)
- Target parameters
  - The largest lateral displacement of the wall (Dis) (mm)

The illustration of factors and Dis plots displayed in Fig. 1 enhances the understanding of the distribution of the data set in a more thorough manner.

The Pearson correlation coefficient (CC_P), is a measure of the strength and direction of a linear relationship between two variables. It ranges from -1 to 1, where CC_P equals 1 indicates a perfect positive linear relationship (increasing one variable raised another), CC_P equals -1 indicates a perfect negative linear relationship (increasing one variable decreased another), and CC_P equals 0 indicates no linear relationship (increasing one variable has no impact on another).

The formula for calculating the CC_P between two variables, X and Y, with n data points is given by

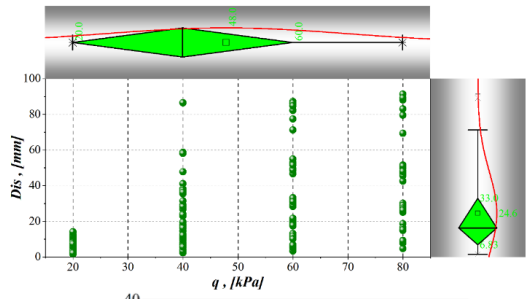

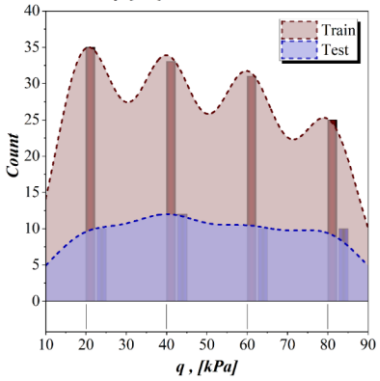

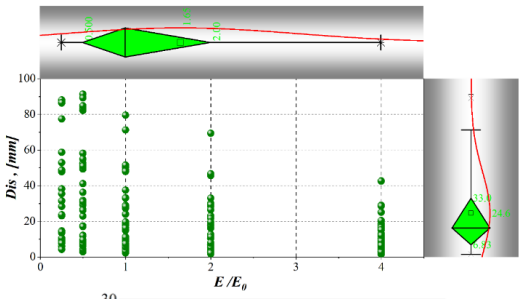

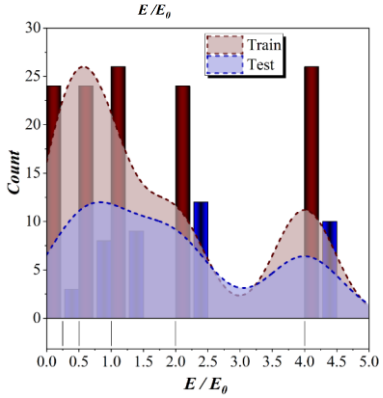

(a) (b)

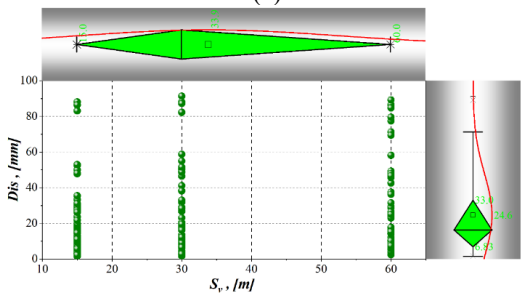

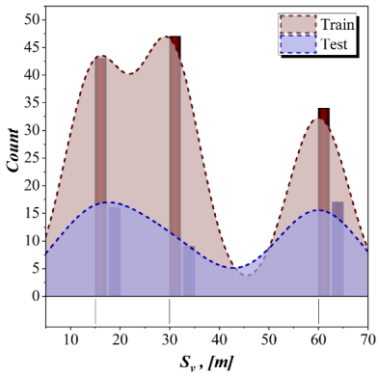

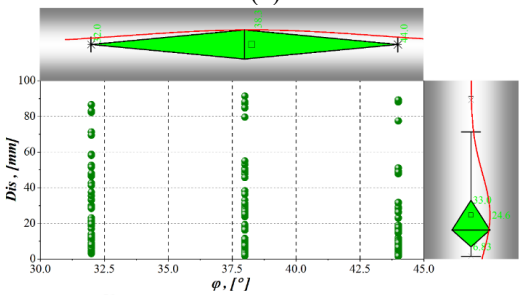

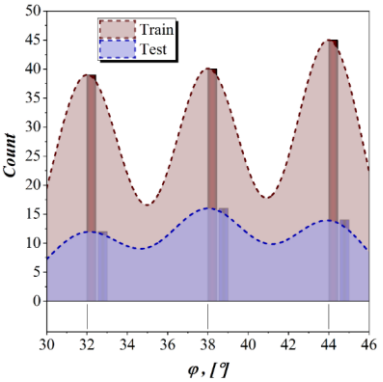

(c) (d)

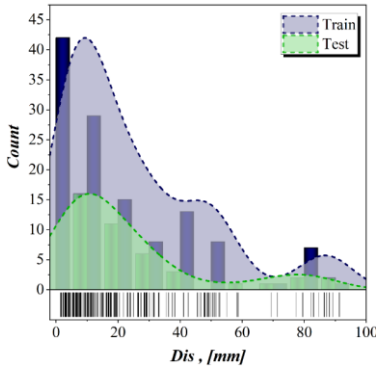

(e)

Fig. 1 The distribution figures of input variables Vs. target

Algorithm 1. The Pseudocode of $AnOA$ (Mirjalili 2015)

Start

- *Initializing the population of ants and antlions*
- *Calculating the objective function values of ants and antlions*
- *Finding the best antlions (local optimal solution)*
- ***while** (the exit criterions are not satisfied)*
- ***for** every ant*
- *Selecting an antlion using roulette wheel mechanism*
- *Updating c and d by Eqs. (2) and (3)*
- *Creating a random walk and normalizing it*
- *Updating the position of ant*
- ***end for***
- *Calculating the objective function values of all ants*
- *Updating local optimal solution by Eq. (5)*
- ***end while***
- ***return** best antlions*

End

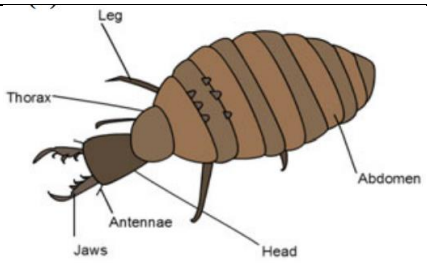

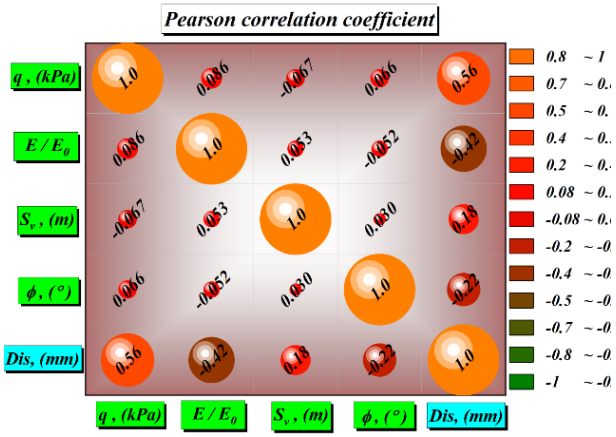

Fig. 2 The values of correlation

$$CC_P = \frac{\sum(I_i - \bar{I})(T_i - \bar{T})}{\sqrt{\sum(I_i - \bar{I})^2 \sum(T_i - \bar{T})^2}} \tag{1}$$

In this equation, I_i and T_i depict the individual data points, and $\bar{I}$ and $\bar{T}$ are the average of I and T, respectively. The CC_P is widely used in statistics to quantify the strength and direction of a linear relationship between two variables. It's important to note that correlation does not imply causation, and the relationship may be influenced by other factors or follow a non-linear pattern. As it is obvious from concluded values of CC_P in Fig. 2, most of the variables has small linear relationship smaller than 0.22. Moreover, the largest but moderate positive relationship is between q, and Dis at 0.56, along with negative moderate CC_P at -0.42 between $E\,/\,E_0$ with Dis . Interestingly, the large correlations are between some parameters and the target, not between variables, where if the model could result higher accuracy by overcoming these impacts, depicting its dependability.

*2.2 Ant lion optimization algorithm (**AnOA**)*

$AnOA$, which is based on the hunting mechanism of ant lions in their nature, has been suggested and demonstrates excellent performance on benchmark functions (Mirjalili 2015). The $AnOA$ method replicates the interplay among antlions and ants inside traps. Antlions navigate across the search area and employ traps to enhance their hunting effectiveness. Ants' foraging activity is inherently stochastic, and their motions are accurately modeled using an arbitrary walk. The movement patterns of ants are influenced by the presence of antlion traps, and this phenomenon may be represented using the given mathematical formulas

$$c^t = \frac{c^t}{10^{\omega} \times \frac{t}{t_{max}}} \tag{2}$$

$$d^t = \frac{d^t}{10^{\omega} \times \frac{t}{t_{max}}} \tag{3}$$

Let c^t represent the smallest value among every parameter at the t_{th} iteration, and let d^t be the vector that contains the largest value among every parameter at the t_{th} iteration. ω represents a function of t that is defined by different formulas for different intervals of t.

$$\omega = \begin{cases} 2, t > 0.1t_{max} \\ 3, t > 0.5t_{max} \\ 4, t > 0.75t_{max} \\ 5, t > 0.9t_{max} \\ 6, t > 0.95t_{max} \end{cases} \tag{4}$$

Upon capturing the prey, antlions will reconstruct the hole by utilizing the subsequent formula

$$Antlions_j^t = Ant_i^t \; if \; f(Ant_i^t). > f\left(Antlion_j^t\right) \tag{5}$$

Let t represent the present iteration. $Antlions_j^t$ represents the locations of the chosen j_{th} antlion at the t_{th} iteration, and Ant_i^t denotes the location of the i_{th} ant at the t_{th} iteration. The pseudocode for the $AnOA$ method is shown in algorithm 1.

2.3 Chimp optimization algorithms ($ChOA$)

The $ChOA$ is a method that is according to swarming and is influenced by the innate hunting behaviors of chimpanzees (Khishe and Mosavi 2020). The population is composed of four distinct groups of agents: the driver, chaser, barrier, and attacker. Every chimpanzee in a community has unique abilities, which are essential for the purpose of hunting. The following are fundamental mathematical explanations of $ChOA$

$$x_{chimp}^{(t+1)} = x_{prey}^t - a \cdot \left| c \cdot x_{prey}^t - m \cdot x_{chimp}^t \right| \tag{6}$$

In this context, "x_{prey}^t" represents the location of the prey, whereas "x_{chimp}^t" represents the position of the chimpanzees. "t" refers to the present iteration, "$\cdot$" represents the element-wise production, and "a", "m", and "c" are coefficient vectors derived using Eqs. (7) to (9).

$$a = 2 \cdot f \cdot rand_1 - a \tag{7}$$

$$c = 2 \cdot rand_2 \tag{8}$$

$$m = Chaotic\_value \tag{9}$$

Let $rand_1$ and $rand_2$ be random values between 0 and 1. The function f is gradually reduced in a non-linear manner over the iterations within the range of 2.5 to 0. The chaotic vector m represents the sexual motives of the agents, which are determined utilizing different chaotic mappings (Khishe and Mosavi 2020). The $ChOA$ starts its process by generating a stochastic collective of people. Chimpanzees are categorized into one of four classes based on their behavior: the attacker, driver, chaser, or barrier. Although every chimpanzee attempts to determine the best position of their victims, the placement of individuals in every group will be revised by calculating the f vector value for every tactic. The current position of the victim is the most optimal so far.

$ChOA$ accepts every continuous function that is modified by autonomous classes and has a decreasing trend over iterations. Fig. 3 displays the two potential selections made for the variable f in four different groups from the analyzed methodologies. In the subsequent portions of this work, the $ChOA_1$ is used. The mathematical models of the employed f vectors may be found in reference (Khishe and Mosavi 2020).

The attacker begins the exploitation stage with assistance from the other chimpanzees. The ideal prey location for modeling hunting manner analytically is determined using the most effective answers found. The most proficient agents are the first attacker, barrier, driver, and chaser. The location update rule is seen as follows

$$x_1 = x_{attacker}^t - a_1 \left| c_1 x_{attacker}^t - m_1 x^t \right| \tag{10}$$

$$x_2 = x_{Barrier}^t - a_2 \left| c_2 x_{Barrier}^t - m_2 x^t \right|$$

$$x_3 = x_{Chaser}^t - a_3 \left| c_3 x_{Chaser}^t - m_3 x^t \right|$$

$$x_4 = x_{Driver}^t - a_4 \left| c_4 x_{Driver}^t - m_4 x^t \right|$$

$$x^{(t+1)} = \frac{x_1 + x_2 + x_3 + x_4}{4} \tag{11}$$

Empirical data suggests that the use of chaotic maps may expedite the resolution of high-dimensional issues and circumvent the issue of local optima. The mathematical models used in this study may be found in reference (Khishe and Mosavi 2020), which describes chaotic maps. Assume that half of the chimpanzees will consistently behave via the latter phase of the search, while the other half will use unpredictable techniques to alter the chimpanzee's location. Eq. (12) denotes the revised mathematical expression for this approach

$$x_{chimp}^{(t+1)} = \begin{cases} x_{prey}^t - a \cdot d & if \quad \mu < 0.5 \\ Chaotic_{value} & if \quad \mu \geq 0.5 \end{cases} \tag{12}$$

where μ is a uniformly distributed accidental variable ranging from 0 to 1, including both endpoints. Consequently, arbitrary chimpanzees are utilized to initiate $ChOA$. Furthermore, every person is assigned to one of the four distinct categories. Agents subsequently revise the f vector via the use of the classified technique. Subsequently, throughout each iteration, the four classes evaluate the likely positions of their prey. Chaotic maps effectively eliminate the occurrence of local minima and accelerate the rate of convergence.

2.4 Gannet optimization algorithm ($GaOA$)

The $GaOA$ represents a novel meta-heuristic method that draws inspiration from the hunting manner of gannets in nature. The process primarily comprises of two distinct stages, namely exploration and exploitation. The exploration stage quantifies the gannet's U- and V-shaped diving methods, while the exploitation stage concentrates on the gannet's abrupt rotation and unpredictable swimming patterns. These two phases are executed alternately to locate the optimal region in the search area.

Initialization Phase

The $GaOA$ begins with a collection of answers X that are arbitrarily started. It then determines whether to engage in an exploration or exploitation stage based on a certain possibility. The $GaOA$ comprises a memory matrix MX. After executing every modify tactics, the existing location is not instantly modified with the novel location discovered. However, the novel location is evaluated against the fitness value of the present location and the individual with the superior fitness value is preserved in the X matrix. The initialization step provides the value of X to the variable MX.

Exploration Phase

During hunting, gannets often survey their target from the sky and strategically select areas with high target density to swiftly dive into the water. Gannets exhibit two

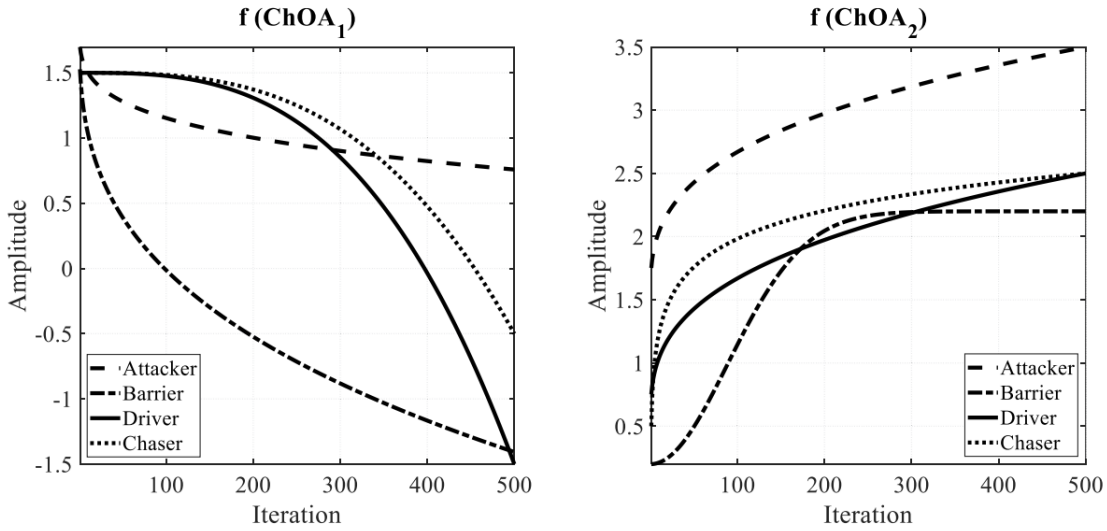

Fig. 3 Mathematical systems of the non-linear decrement of f vectors (Bo *et al*. 2023)

distinct styles of diving after swiftly entering the water: U-shaped and V-shaped dives (Fig. 4). A U-shaped dive is characterized by a lengthy and profound descent, whereas a V-shaped dive is characterized by a brief and shallow descent. Eq. (13) reflects the U-shaped dive of the gannet, whereas Eq. (14) describes the V-shaped dive.

$$a = 2 \times \cos(2 \times \pi \times r_1) \times t \tag{13}$$

$$b = \times V(2 \times \pi \times r_2) \times t \tag{14}$$

$$t = 1 - \frac{It}{T_{mam-iter}} \tag{15}$$

$$V(x) = \begin{cases} -\frac{1}{\pi} \times x + 1, x \in (0, \pi) \\ \frac{1}{\pi} \times x - 1, x \in (\pi, 2\pi) \end{cases} \tag{16}$$

The variables r_1 and r_2 represent arbitrary values that range among 0 and 1. The present amount of iterations is shown by It, while $T_{mam-iter}$ is the highest number of iterations provided. It is evident that t gradually reduces over the iterations till it approaches a value of 0.

After the two dive forms are established, the gannet adjusts its locations based on these shapes. To determine diving shape the gannet picks while feeding, an arbitrary number q is assigned with equal chance to each dive form.

$$MX_i(t+1) = \begin{cases} X_i(t) + u1 + u2, & q \geq 0.5 \\ X_i(t) + v1 + v2, & q < 0.5 \end{cases} \tag{17}$$

$$u2 = A \times \left(X_i(t) - X_r(t)\right) \tag{18}$$

$$v2 = B \times \left(X_i(t) - X_m(t)\right) \tag{19}$$

$$A = (2 \times r_3 - 1) \times a \tag{20}$$

$$B = (2 \times r_4 - 1) \times b \tag{21}$$

Let $u1$ and $v1$ represent random integers within the range of $[-a, a]$ and $[-b, b]$, accordingly. $X_i(t)$ refers to the i^{th} individual in the present populace, $X_r(t)$ represents an arbitrarily chosen individual from the present populace, and $X_m(t)$ denotes the mean location of all individuals in the present populace. r_3 and r_4 are randomly generated decimal values ranging from 0 to 1.

Exploitation Phase

During a gannet's hunting activity in the water, a nimble fish often executes an abrupt maneuver to evade capture. The capture capacity is quantified by a variable C, that diminishes as the number of repetitions increases (as shown in Eq. (22)). The variable cf represents the centripetal force exerted by the fish in the water.

$$C = \frac{1}{cf \times t2} \tag{22}$$

$$t2 = 1 + \frac{It}{Tmax - iter} \tag{23}$$

$$cf = \frac{M \times vs.el^2}{L} \tag{24}$$

$$L = 0.2 + (2 - 0.2) \times r_5 \tag{25}$$

The gannet's weight in actuality is 2.5 kg, and its dive speed in the water is 1.5 m/s. Additionally, r_5 represents an arbitrary number ranging from 0 to 1.

Specify a constant c. If the gannet's capture ability C is sufficient (more than or equal to c), the method will implement a quick turn tactic to modify the gannet's present location. Alternatively, this implies that the gannet lacks the energy to successfully chase the clever fish at now. As a result, it resorts to the tactic of aimless roaming in order to refresh its location, as described by Eq. (26).

$$MX_i(t+1) = \begin{cases} t \times delta \times \left(X_i(t) - X_{Best}(t)\right) + X_i(t), & C \geq c \\ X_{Best}(t) - \left(X_i(t) - X_{Best}(t)\right) \times P \times t, & C < c \end{cases} \tag{26}$$

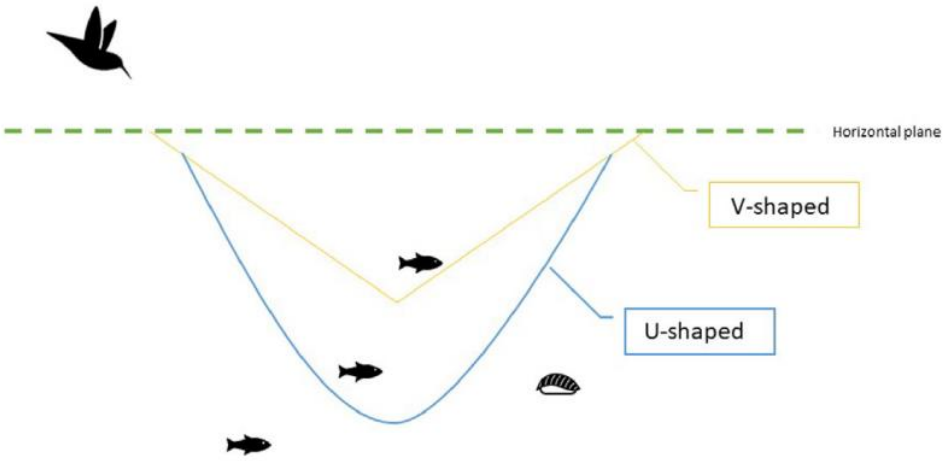

Fig. 4 V- and U-shaped (Pan *et al.* 2022)

Algorithm 2. Pseudo-code of the $GaOA$ (Pan *et al*. 2022)

Start

Input:

N: population size

Dim: problem dimension

$T_{max-iter}$*: maximum number of iterations*

- *Initialize the population X randomly, r and q are all random numbers from 0 to1*
- *Generate memory matrix MX*
- *Calculate the fitness value of X*
- ***while*** *stopping condition is not met* ***do***
- ***if*** $r > 0.5$ ***then***
- ***for*** MX_i ***do***
- ***if*** $q \geq 0.5$ ***then***
- *Update the location Gannet using Eq. (17), where* $q \geq 0.5$
- ***else***
- *Update the location Gannet using Eq. (17), where* $q < 0.5$
- ***end if***
- ***end for***
- ***else***
- ***for*** MX_i ***do***
- ***if*** $C \geq 0.2$ *then*
- *Update the location Gannet using Eq. (26), where* $C \geq 0.2$
- ***else***
- *Update the location Gannet using Eq. (26), where* $C < 0.2$
- ***end if***
- ***end for***
- ***end if***
- ***for*** MX_i ***do***
- *Calculate the fitness value of* MX_i
- ***if*** *the value of* MX_i *is better than the value of* X_i*, replace* X_i *with* MX_i
- ***end for***
- ***end while***

Output: *the position of the best individual and its fitness value*

End

$$delta = C \times |X_i(t) - X_{Best}(t)| \quad (27)$$

$$P = Levy(Dim) \quad (28)$$

The finest individual in the present populace is denoted as $X_{Best}(t)$, and $Levy()$, the individuals' manner roaming arbitrarily is modeled using the Levy flight function, that is defined in Eq. (29).

$$Levy(Dim) = 0.01 \times \frac{\mu \times \sigma}{|v|^{\frac{1}{\beta}}} \quad (29)$$

$$\sigma = \left(\frac{\Gamma(1+\beta)\sin\left(\frac{\pi\beta}{2}\right)}{\Gamma\left(\frac{1+\beta}{2}\right) \times \beta \times 2^{\left(\frac{\beta-1}{2}\right)}} \right)^{\frac{1}{\beta}} \quad (30)$$

Here, $\mu \sim N, vs. \sim N(0,1)$, The value of β is pre-determined as 1.5. Γ is the gamma function, and Dim represents the dimensional size of the issue. The $GaOA$ has two distinct phases: exploration and exploitation, with every stage including two modify techniques. Algorithm 2 presents the pseudo-code for the $GaOA$.

*2.5 Random Forests (**RF**) regression*

RF is a method that is merged with other methods, as stated by (Ge *et al.* 2022). In integrated approaches, the selected model for classification or regression is a composite of many models. Every model cast its own vote, and the ultimate outcome is determined according to the aggregated values of these votes. The precision of an integrated technique is often superior to that of its individual components (Fan *et al*. 2022). Consider a scenario where the models utilized in the integration approach consist only of decision tree kinds. Consequently, this collection of models will constitute a forest. Every decision tree is built by randomly selecting certain qualities at every node to decide the branch. Put simply, every tree is built using the values of a random vector. The dispersion of these values is consistent across every tree in the forest and they are sampled in an independent manner. During the categorization process, every tree contributes its vote, and the ultimate outcome is chosen by a majority vote (Liaw and Wiener 2002).

The RF method's crucial variables are the number of parameters chosen at every node in the tree and the number of trees for which suitable values must be determined. This approach involves swapping data throughout every sampling process, resulting in some information being excluded from sampling while others may be sampled multiple times. Put simply, some input data for certain trees will be excluded from the bag, referred to as out-of-bag (OOB), indicating that they will not be used in the creation of those trees. This data serves as an internal validator for every tree, that is verified by predicting the inaccuracy outside the bag. Using trees to forecast the out-of-bag data will result in errors in these forecasts. The out-of-bag error refers to the mean of these faults and it quantifies the impact of unselected samples on the ultimate fault rate of the RF. The RF method operates by the following sequential procedures:

• Randomly selecting N data points from the dataset,

• Create a decision tree using the chosen dataset,

• Specify the required quantity of trees and then redo the previous two procedures,

• Resolve the regression quandary by having every decision tree provide a value as its result. The ultimate value may be determined by computing the mean of the results from every tree for every dataset.

The RF model is widely regarded as a robust benchmark model due to its simplicity and reliability. Its use allows researchers to evaluate whether the added complexity of advanced models, such as boosting algorithms, leads to meaningful performance improvements. Furthermore, RF exhibits resilience to overfitting by aggregating predictions from multiple decision trees, making it a dependable choice for datasets containing noise or outliers. Compared to gradient boosting methods, RF often offers greater interpretability, with feature importance scores providing clear insights into the influence of input variables on predictions. Additionally, RF is computationally efficient for small to medium-sized datasets, making it a practical option when computational resources are constrained. Unlike sequential boosting models, RF constructs multiple trees independently, enabling parallel implementation and reducing training time. Lastly, in scenarios where the marginal performance gains from advanced models are minimal, RF can deliver sufficient accuracy while maintaining lower complexity, making it a valuable predictive tool in various contexts.

The present study used the RF regression method to elucidate the non-linear correlation between the variables. The four essential RF hyperparameters, which are critical for learning and indispensable for achieving exceptional performance (Qi *et al*. 2018), were determined (tunned) by $AnOA$, $ChOA$, and $GaOA$ algorithms. these hyperparameters are: a) $Max\_Depth \rightarrow Max_D$: The highest depth of decision trees, b) $Min\_Samples\_Split \rightarrow Min_{SS}$: The lower number of split samples, c) $Max\_DT \rightarrow Max_{DT}$: The highest number of RT in the ensemble, and d) $Max\_Features \rightarrow Max_F$: The number of features considered during the selection of the best splitting. To mitigate the uncertainty of random splitting, five RF simulations were constructed for each set of parameters inside the Python software domain. The modification of all variables in the optimization algorithms was determined via the process of trial and error. The locations were adjusted to get the highest possible fitness value, while also adjusting the hyperparameters that were taken into account. This was done by repeating the optimization procedures. Ultimately, during the testing phase, the RF models with the optimal hyperparameters was validated (Table 2).

2.6 Performance evaluation metrics

An important stage of the framework design process is the validation and evaluation of the models that have been developed. After the simulation is finished, a validation procedure must be carried out to make sure the models are

accurate and, as a result, maximize their potential to meet the goals that were originally planned. Utilizing data from training and testing sets, the effectiveness of each of the aforementioned strategies has been assessed (Aghayari Hir *et al.* 2022). Eleven statistical metrics were utilized to evaluate the accuracy and reliability of the models carried out in this study (Eqs. (31)-(41)).

$$R^2 = \left(\frac{\sum_{g=1}^{G} (n_g - \bar{n})(z_g - \bar{y})}{\sqrt{\left[\sum_{g=1}^{G} (n_g - n)^2\right]\left[\sum_{g=1}^{G} (y_g - \bar{y})^2\right]}} \right)^2 \quad (31)$$

$$RMSE = \sqrt{\frac{1}{G}\sum_{g=1}^{G} (y_g - n_g)^2} \quad (32)$$

$$\text{NRMSE} = \text{RMSE}/\bar{y} \quad (33)$$

$$MAE = \frac{1}{G}\sum_{g=1}^{G} |y_g - n_g| \quad (34)$$

$$TIC = \frac{\sqrt{\frac{1}{G}\sum_{g=1}^{G} (y_g - n_g)^2}}{\left(\sqrt{\frac{1}{G}\sum_{g=1}^{G} y_g{}^2} + \sqrt{\frac{1}{G}\sum_{g=1}^{G} n_g{}^2}\right)} \quad (35)$$

$$IA = 1 - \frac{\sum_{g=1}^{G} (n_g - y_g)^2}{\sum_{g=1}^{G} (|n_g - \bar{n}| + |y_g - \bar{n}|)^2} \quad (36)$$

$$NMSE = \frac{1}{G}\sum_{g=1}^{G} \left(\frac{n_g - y_g}{SD}\right)^2 \quad (37)$$

$$A_{10} = \frac{g_{10}}{G} \quad (38)$$

$$Un_{95} = 1.96\sqrt{(SD^2 + RMSE^2)} \quad (39)$$

$$SI = \frac{\sqrt{\left(\frac{1}{G}\right)\sum_{g=1}^{G} ((n_g - \bar{n}) - (y_g - \bar{y}))^2}}{\left(\frac{1}{G}\right)\sum_{g=1}^{G} y_g} \quad (40)$$

$$OBJ = \frac{n_{train}}{D}\left(\frac{RMSE_{Train} + MAE_{Train}}{R^2_{Train} + 1}\right) + \frac{n_{test}}{D}\left(\frac{RMSE_{Test} + MAE_{Test}}{R^2_{Test} + 1}\right) \quad (41)$$

In these equations, n_g, $\bar{n}$, y_g, and $\bar{y}$ present the actual Dis, mean of the actuals, the estimated Dis, and the mean of the estimations, respectively. G is the number of the data points. Herein, g_{train} and g_{test} present the number of data points in the learning, and examining subsets, respectively. SD is the abbreviation form of the standard deviation. The term g_{10} is the number of estimated/actual ratio between 0.9 and 1.1.

3. Findings and justifications

In order to create the linked RF designs, the following steps were completed:

- The first step was setting up the original RF version.
- The generated data points were then partitioned into two subsets for the purposes of learning, and examining, using a randomization technique.
- Afterwards, the RF models that were set up were coupled with the optimization techniques called $AnOA$, $ChOA$, and $GaOA$, resulting in $RF(AnOA)$, $RF(ChOA)$, and $RF(GaOA)$ respectively.
- Once the required target function was obtained, an examination was conducted to determine the optimal values for each algorithm's hyperparameters (Table 2).

This paper presents the results gained by integrating the $AnOA$, $ChOA$, and $GaOA$ processes with hybrid and RF approaches. The deformation properties (Dis) of soil structures reinforced with geogrid have been identified utilizing the earlier described procedures. Fig. 5 displays the anticipated and actual Dis values for each of the three distinct hybrid RF techniques, namely $RF(AnOA)$, $RF(ChOA)$, and $RF(GaOA)$, during the learning and examination stages. Furthermore, the picture provided displays the percentage distribution of error. The prediction effectiveness of the algorithms for Dis was assessed using a number of metrics, namely R^2, $RMSE$, $NRMSE$, MAE, TIC, IA, $NMSE$, $A10$, U_{95}, and SI, as well as a comprehensive indicator called OBJ. Furthermore, a scoring system has been devised for each index associated with each design, with the highest score indicating the best suitable option. Table 3 presents a comprehensive overview of the results obtained from the measurements included in the models. It notably emphasizes the optimal situation and the corresponding scores attained throughout the learning and evaluation parts. Moreover, this research aims to determine the effectiveness of the designs by comparing the results with those of a prior publication (Momeni et al., 2021).

Based on the data, the $RF(AnOA)$, $RF(ChOA)$, and $RF(GaOA)$ methods have a significant ability to accurately predict the Dis of $GSRW$. During the learning and examination stages, the R^2 values for the $RF(GaOA)$ net were found to be 0.9823 and 0.9943, respectively. When compared to the $RF(ChOA)$, which had R^2 values of 0.9845 and 0.9884, and the $RF(AnOA)$, which had R^2 values of 0.9761 and 0.9727, respectively, these values were bigger. Throughout the estimating phases, all of the models demonstrated high performance and accuracy levels. Other error-based measurements, such as $RMSE$, $NRMSE$, MAE, TIC, and $NMSE$, may be helpful in determining the approach's accuracy. These indices' values show that $RF(GaOA)$ outperforms $RF(ChOA)$ and $RF(AnOA)$, with the latter two showing a remarkable difference. For instance, the value of TIC was 0.0463 and 0.0282 in the learning and examining sections for $RF(GaOA)$, remarkably smaller than those of $RF(ChOA)$ at 0.0523 and 0.063, and $RF(AnOA)$ by 0.0564 and 0.0799,

Table 2 The considered and optimal values for optimization algorithms and hybrid RFs

Optimization algorithms	Initial parameters	Value	Hybrid RF	Hyperparameters	Value
$AnOA$	Number of iterations	200	$RF(AnOA)$	Max_D	25
	Number of runs	10		Min_{SS}	3
	Ants' pop. size	20		Max_{DT}	202
	Ant lions' pop. size	20		Max_F	0.882
$ChOA$	Number of iterations	200	$RF(ChOA)$	Max_D	32
	Number of runs	10		Min_{SS}	3
	Population number	20		Max_{DT}	104
	f_{r1}	Non-linearly decreased from 2.5 to 0		Max_F	0.705
	r_{2m}	Random [0, 1]			
$GaOA$	Number of iterations	200	$RF(GaOA)$	Max_D	21
	Number of runs	10		Min_{SS}	2
	Population number	20		Max_{DT}	83
	Weight of the gannet M	2.5		Max_F	0.536
	Gannet speed Vel	1.5			
	c	0.2			
	Constant in Levy flight function	1.5			

Table 3 The metrics-based evaluation of hybrid RF frameworks

Stage	Metrics	Models (This study)						(Momeni et al., 2021)
		$RF(AnOA)$	Point	$RF(GaOA)$	Point	$RF(ChOA)$	Point	ANN^{GSA}
$Train$	R^2	0.9761	10×1	0.9823	10×3	0.9845	10×2	0.9643
	$RMSE$	3.8246		3.1661		3.524		
	$NRMSE$	0.1518		0.1252		0.1397		
	MAE	2.3782		1.7045		2.115		
	TIC	0.0564		0.0463		0.0523		
	IA	0.9928		0.9952		0.9937		
	$NMSE$	0.0179		0.0044		0.016		
	$A10$	0.5403		0.8468		0.6129		
	U_{95}	10.6209		8.7938		9.7868		
	SI	0.1511		0.1251		0.1393		
$Test$	R^2	0.9727	10×1	0.9943	10×3	0.9884	10×2	0.9702
	$RMSE$	4.887		1.794		3.8748		
	$NRMSE$	0.225		0.0802		0.1774		
	MAE	2.7353		1.0172		2.2497		
	TIC	0.0799		0.0282		0.063		
	IA	0.9866		0.9984		0.9917		
	$NMSE$	0.0193		0.0042		0.0164		
	$A10$	0.5		0.9048		0.619		
	U_{95}	13.5689		5.003		10.7547		
	SI	0.2185		0.0802		0.1732		
Summated points			20		60		40	
OBJ		3.3223		2.192		2.9019		

respectively. The values of $NMSE$ index were notable, where almost 75% decline was observed for $RF(GaOA)$ with respect to others. Based on the metrics provided in this study for the built models, $RF(GaOA)$ might have higher values than other systems where $RF(ChOA)$ and $RF(AnOA)$ results are almost identical. Last but not least, $RF(GaOA)$ has the lowest value, 2.192 (Score at 60), compared to $RF(ChOA)$ at 2.9019 (Score at 40) and $RF(AnOA)$ by 3.3223 (Score 20) in relation to the OBJ index and the summed-up ratings.

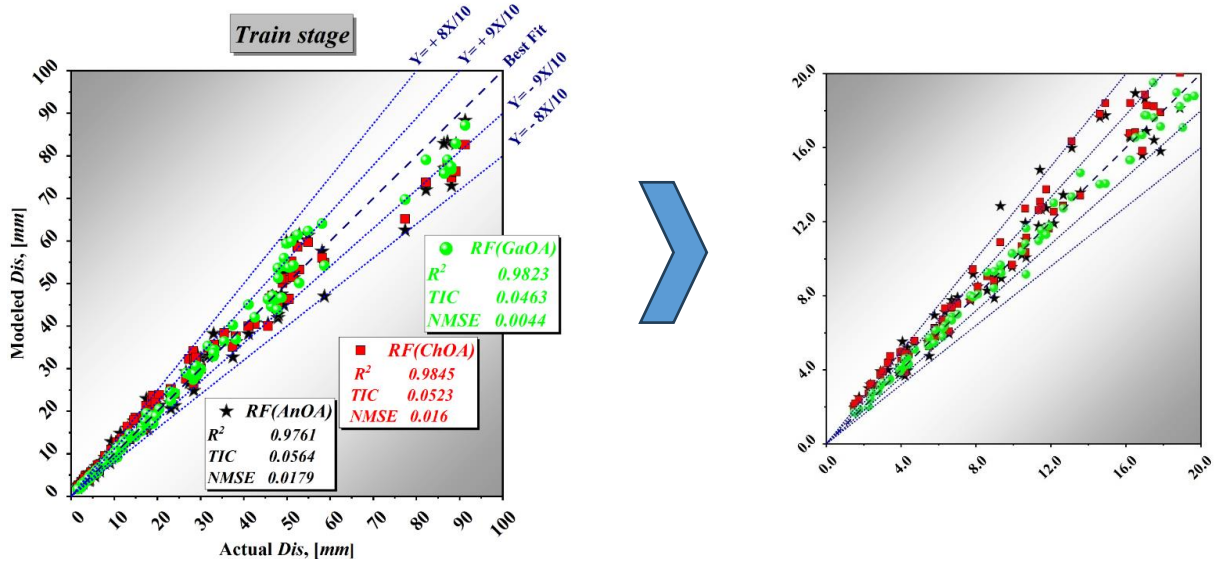

(a)

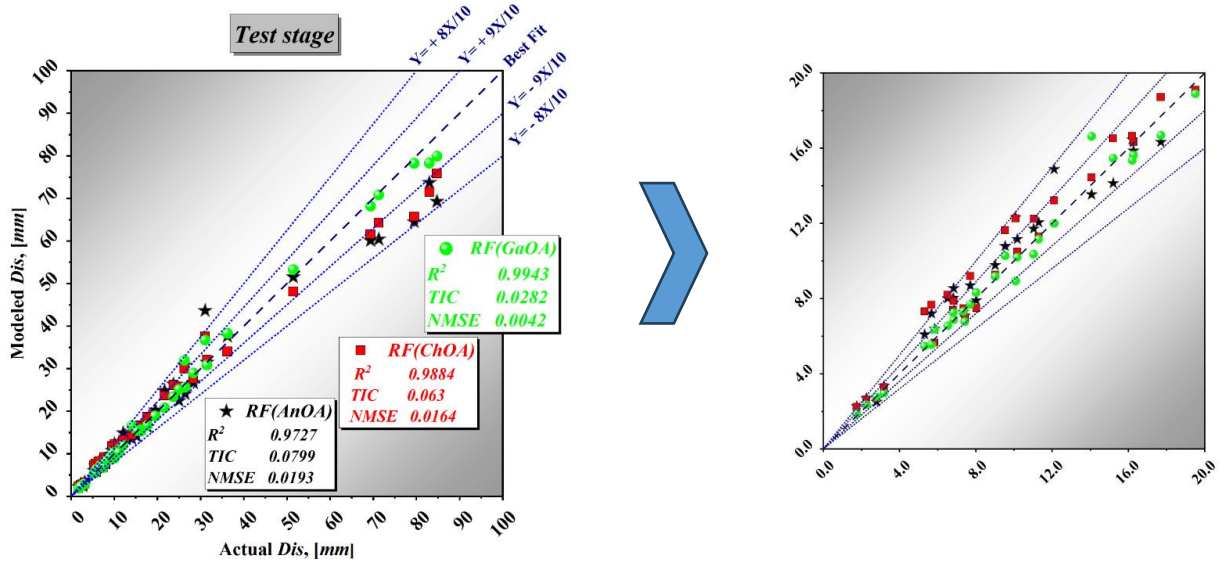

(b)

Fig. 5 The scatter plots of correlation for developed models versus actual Dis

The results of the modifiability investigators referred to as Un_{95}, are shown in Table 3. It should be noted that a greater level of generalization competency is associated with a lower value of Un_{95} (Behar *et al.* 2015, Gueymard 2014). It is evident that the lower values of Un_{95} held by $RF(GaOA)$ in subgroups are 8.7938 and 5.003 for learning and examining sections, respectively. These values are smaller when compared with those of $RF(ChOA)$ and $RF(AnOA)$. The effectiveness of $RF(ChOA)$, and $RF(AnOA)$ is roughly identical with a slight superiority of $RF(ChOA)$ (by 9.7868, and 10.7547 for learning and examining portions, respectively) with respect to $RF(AnOA)$ (at 10.6209, and 13.5689 for learning and examining portions, respectively). The arguments presented generally indicate that the $RF(GaOA)$ analysis can do more than the $RF(ChOA)$ and $RF(AnOA)$ analyses.

An extensive evaluation of the reliability of the simulations is conducted by a comparative analysis with a previously published scholarly work (Momeni *et al.* 2021).

Upon meticulous examination of Table 3, it is evident that the $RF(GaOA)$ algorithm, created in this study, yielded superior outcomes compared to the previous trials documented in the existing literature. The assessment was conducted using a standardized metric called R^2, which was consistently used throughout both the learning and examining phases. Throughout the learning stage, the R^2 value shows a rise from 0.9643 (ANN^{GSA}) to 0.9823. Similarly, during the examining stage, there is a rise from 0.9702 (ANN^{GSA}) to 0.9943.

Fig. 6 displays the distribution of errors in prediction across the three RF-based approaches throughout both the learning and examining periods. Improvement in efficiency can be observed by a limited band of error %, including both a smaller and larger threshold. The findings indicate

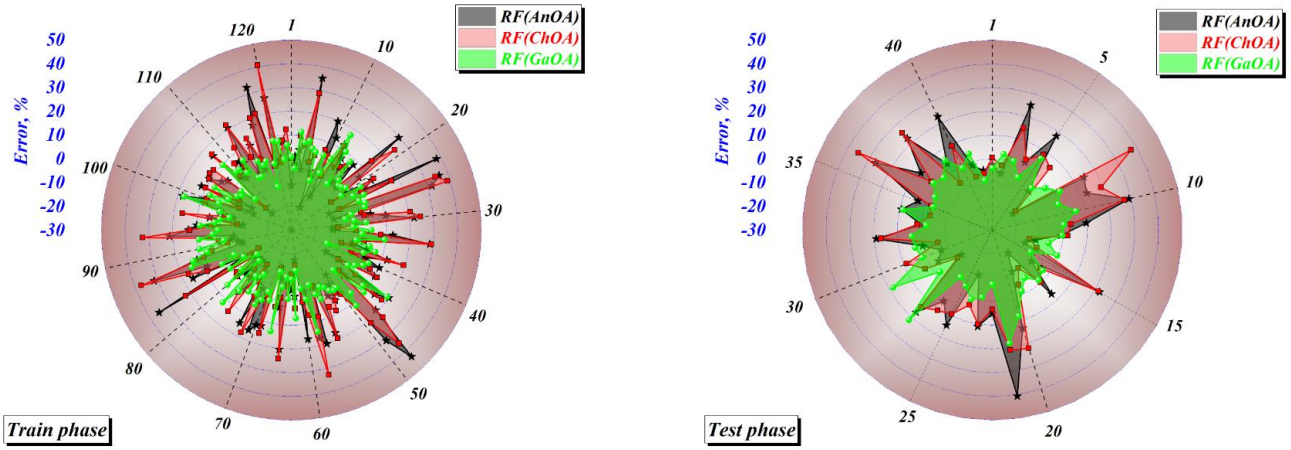

Fig. 6 Error percentage distribution in the train and test phases

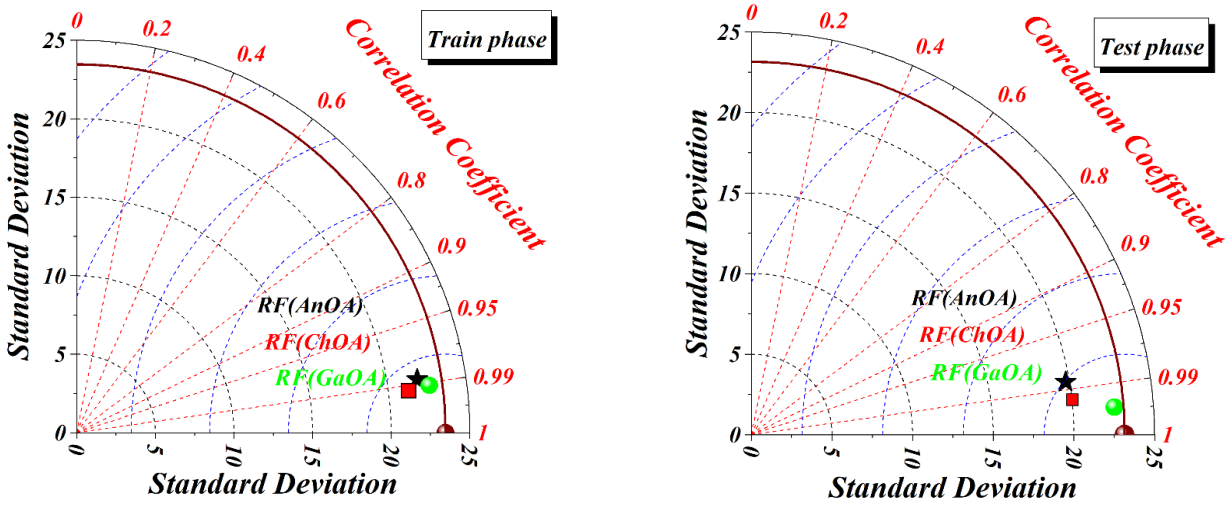

Fig. 7 Taylor diagram

that $RF(AnOA)$ has worse efficacy at different phases, as shown by a greater degree of variability in errors. Subsequently, the variant known as $RF(ChOA)$ was shown to be the second least effective version. When the $GaOA$ method is used to improve the RF approach, it exhibits a notable occurrence of errors, especially in cases when the error rate near zero and is limited to certain criteria

The primary objective of Taylor diagram analysis is to visually and quantitatively evaluate the level of agreement between a set of data or simulation of a model and a benchmark data. The Taylor diagram can be employed to evaluate many crucial facets of the model's efficacy simultaneously. The components encompass; Correlation, Standard deviation ratio, and $RMSE$. The Taylor diagram simplifies the comparison of many simulations against a shared set of reference data by consolidating several measures into a single visual representation. The learning and examining subgroups each presented the outcomes of the Taylor diagram for developed models (Fig. 7). The closer position of the model to the base point, the higher accuracy. The shown charts clearly indicate that $RF(GaOA)$ is closer to the reference point than $RF(ChOA)$ and $RF(AnOA)$ while learning and analyzing subsets. This suggests that $RF(AnOA)$ demonstrates its effectiveness in the estimating process.

3.1 Sensitivity analysis

Sensitivity analysis was implemented in this study to assess how input factors affected efficacy. To improve model optimization, comprehension, and decision-making, sensitivity analyses carried out in simulation studies provide a systematic manner to comprehend the effects of variables on the efficacy of analysis. The present study included the development of several hypotheses, each employing unique inputs in an effort to increase the performance of the validated system ($RF(GaOA)$). Unlike the $RF(GaOA)$ paradigm, the study employed R^2, and TIC measurements to assess the impact of various inputs. Fig. 8 presents the learning and examining portions of the sensitivity analysis results. The greater the impact of missing components on the outcome, the more discrepancies there are in the measures. As compared to $RF(GaOA)$, the results indicate that the absence of all parameters (q, E / E_0, S_v, and φ)

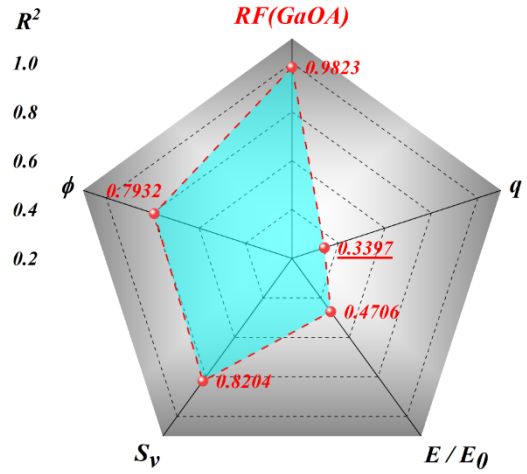

A1- (Train)

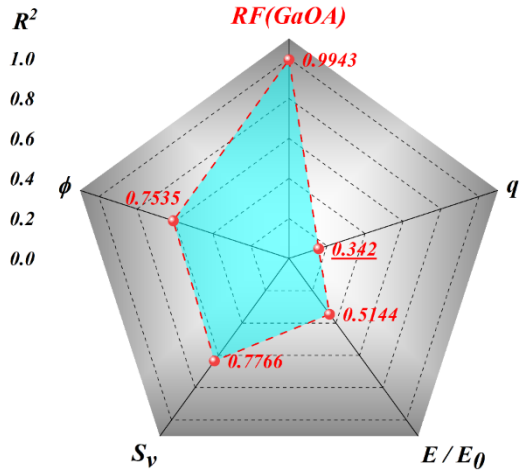

A2- (Test)

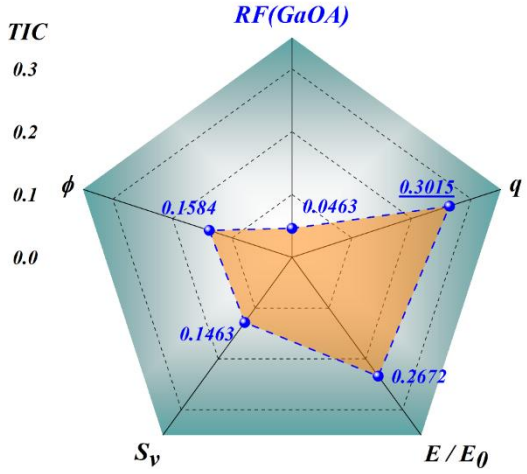

B1- (Train)

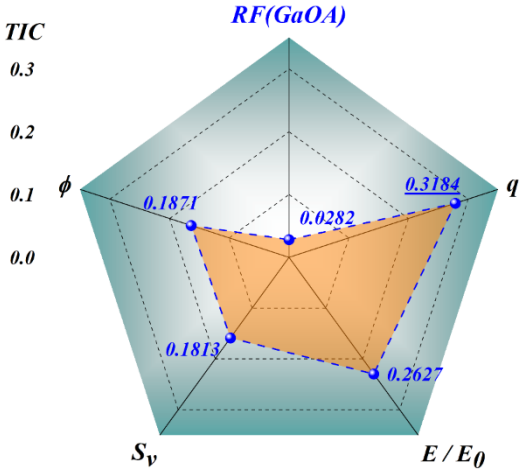

B2- (Test)

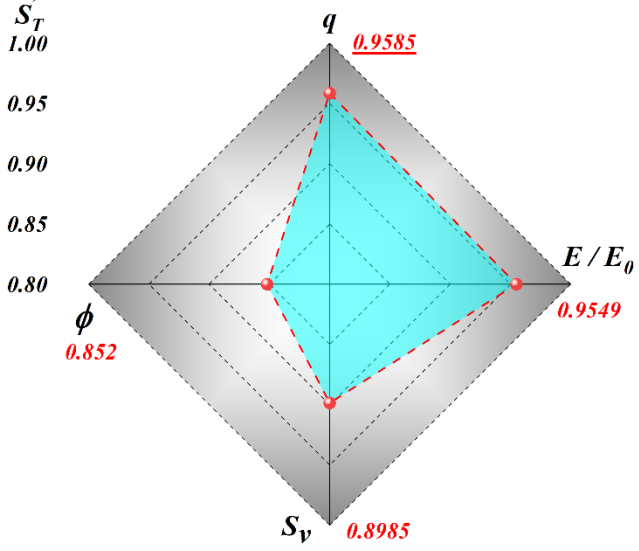

C1-Feature importance-related values using *FAST* methodology

Fig. 8 The results of sensitivity analysis on R^2 and TIC respect to $RF(GaOA)$

significantly worsens the result. Remarkably, there is a large drop in the value of R^2 along with a noticeable rise in the values of TIC when the q parameter is removed from the input group. In the learning stage, the R^2 values showed a drop from 0.9823 to 0.3397, and in the examining stage, from 0.9943 to 0.342. Also, during the learning period, there was a notable increase in TIC from 0.0463 to 0.3015, and during the examining phase, from 0.0282 to 0.3184.

Since the designs were created utilizing analytical data, it is crucial to understand that their comprehensiveness and reliability might be compromised by excluding any input.

Along with this, the results are compared with another feature importance analysis called $FAST$. The results were roughly similar with higher importance of the q at 0.9585, followed by $E\ /\ E_0$ at 0.9549. Next, the S_v, and φ depicted the third and fourth significancy by 0.8985, and 0.852.

3.2 Restriction and future suggestions

Research may be conducted to forecast and analyze the long-term displacement behavior of soil structures that are reinforced by geogrids. This could involve the ongoing surveillance of tangible structures in real-life environments for extended periods of time. The developed algorithms can be utilized for forecasting deformation in geogrid-reinforced soil structures seen in real-life situations. Subsequently, the prediction may be juxtaposed with on-site data to assess the pragmatic viability and efficacy of these models. Integrating reliability analysis into systems is crucial for engineering applications since it enables the calculation of confidence intervals for predictions, hence increasing their worth.

The research is praised for its use of a more extensive dataset compared to prior examinations. Nevertheless, it is possible that employing larger samples might result in further insights and enhance the practicality of the models. The study findings could show uniqueness to the distinct soil and geogrid conditions that comprised the dataset. Performing a comprehensive assessment of the models' efficacy over a wider range of soil types, geogrid designs, and environmental conditions might provide valuable insights.

4. Conclusions

Although multiple designs have been proposed, there is a dearth of dedicated study on the investigation of Random Forests (RF) for estimating deformation (Dis) in geogrid reinforced soil walls ($GRSW$). This study presents and verifies a novel methodology that integrates the ant lion optimization ($AnOA$), Chimp optimization algorithm ($ChOA$), and Gannet optimization algorithm ($GaOA$) with the RF framework for the purpose of identifying appropriate hyperparameters (referred to as $RF(AnOA), RF(ChOA), and\ RF(GaOA)$). The main findings are as below:

• Based on the data, the $RF(AnOA)$, $RF(ChOA)$, and $RF(GaOA)$ methods have a significant ability to accurately predict the Dis of $GSRW$. During the learning and examination stages, the R^2 values for the $RF(GaOA)$ net were found to be 0.9823 and 0.9943, respectively. When compared to the $RF(ChOA)$, which had R^2 values of 0.9845 and 0.9884, and the $RF(AnOA)$, which had R^2 values of 0.9761 and 0.9727, respectively, these values were bigger.

• Error-based measurements' values show that $RF(GaOA)$ outperforms $RF(ChOA)$ and $RF(AnOA)$, with the latter two showing a remarkable difference. For instance, the value of TIC was 0.0463 and 0.0282 in the learning and examining sections for $RF(GaOA)$, remarkably smaller than those of $RF(ChOA)$ at 0.0523 and 0.063, and $RF(AnOA)$ by 0.0564 and 0.0799, respectively.

• $RF(GaOA)$ has the lowest value, 2.192 (Score at 60), compared to $RF(ChOA)$ at 2.9019 (Score at 40) and $RF(AnOA)$ by 3.3223 (Score 20) in relation to the OBJ index and the summed-up ratings.

It was evident that the lower values of Un_{95} held by $RF(GaOA)$ in subgroups are 8.7938 and 5.003 for learning and examining sections, respectively. These values are smaller when compared with those of $RF(ChOA)$ and $RF(AnOA)$. The effectiveness of $RF(ChOA)$, and $RF(AnOA)$ was roughly identical with a slight superiority of $RF(ChOA)$.

• The Taylor diagram charts clearly indicated that $RF(GaOA)$ was closer to the reference point than $RF(ChOA)$ and $RF(AnOA)$ while learning and analyzing subsets.

• As compared to $RF(GaOA)$, the results of sensitivity analysis indicated that the absence of all parameters significantly worsens the result. Remarkably, there is a large drop in the value of R^2 along with a noticeable rise in the values of TIC when the surcharge (q) parameter is removed from the input group. Since the designs were created utilizing analytical data, it is crucial to understand that their comprehensiveness and reliability might be compromised by excluding any input.

• This research provides a significant contribution by establishing a scalable and efficient framework for evaluating the deformation performance of $GRSW$ structures, bridging the gap between computational geomechanics and machine learning. The proposed RF models can replace or complement traditional numerical methods for estimating $GRSW$ deformation, saving time and computational resources. Using these models, engineers can predict $GRSW$ deformations with high precision, enabling more accurate design and better safety assessments of geotechnical structures.

References

Adams, M., Nicks, J., Stabile, T., Schlatter, W. and Hartmann, J. (2012), "Geosynthetic reinforced soil integrated bridge system interim implementation guide", Federal Highway Administration (US).

Afkhami Hoor, S. and Esmaeili-Falak, M. (2024), "Innovative approaches for mitigating soil liquefaction: A state-of-the-art review of techniques and bibliometric analysis", *Indian Geotech. J.*, 1-28. https://doi.org/10.1007/s40098-024-01120-3.

Aghayari Hir, M., Zaheri, M. and Rahimzadeh, N. (2022), "Prediction of rural travel demand by spatial regression and artificial neural network methods (Tabriz County)", *J. Transport. Res.*, https://doi.org/10.22034/tri.2022.312204.2970.

Alias, R., Kasa, A. and Matlan, S.J. (2017), "Comparison of ANN and ANFIS models for stability prediction of cantilever reinforced concrete retaining walls", *Int. J. Eng. Adv. Technol.*, **7**(2), 165-167.

Allen, T.M., Bathurst, R.J. and Berg, R.R. (2002), "Global level of safety and performance of geosynthetic walls: an historical perspective", *Geosynth. Int.*, **9**(5-6), 395-450. https://doi.org/10.1680/gein.9.0224.

Armaghani, D.J., Mirzaei, F., Shariati, M., Trung, N.T., Shariati, M. and Trnavac, D. (2020), "Hybrid ANN-based techniques in

predicting cohesion of sandy-soil combined with fiber", *Geomech. Eng.*, **20**(3), 191-205. https://doi.org/10.12989/gae.2020.20.3.191.

Bathurst, R.J., Miyata, Y. and Allen, T.M. (2010), "Facing displacements in geosynthetic reinforced soil walls", *Earth Retention Conference*, **3**, 442-459. https://doi.org/10.1061/41128(384)45.

Behar, O., Khellaf, A. and Mohammedi, K. (2015), "Comparison of solar radiation models and their validation under Algerian climate–The case of direct irradiance", *Energ. Convers. Management*, **98**, 236-251. https://doi.org/10.1016/j.enconman.2015.03.067.

Berg, R.R., Samtani, N.C. and Christopher, B.R. (2009), "Design of mechanically stabilized earth walls and reinforced soil slopes–Volume II. United States", Department of Transportation. Federal Highway Administration.

Bo, Q., Cheng, W. and Khishe, M. (2023), "Evolving chimp optimization algorithm by weighted opposition-based technique and greedy search for multimodal engineering problems", *Appl. Soft Comput.*, **132**, 109869. https://doi.org/10.1016/j.asoc.2022.109869.

Carter, L. and Bernardi, M. (2014), "NCMA's Design Manual for Segmental Retaining Walls. *Geosynthetics*, **32**(1).

Chen, H., Asteris, P.G., Jahed Armaghani, D., Gordan, B. and Pham, B.T. (2019), "Assessing dynamic conditions of the retaining wall: developing two hybrid intelligent models", *Appl. Sci.*, **9**(6), 1042. https://doi.org/10.3390/app9061042.

Chien-Ta, C., Shing-Wen, T. and Hsiao, L.H. (2024), "Estimating deformation of geogrid-reinforced soil structures using hybrid LSSVR analysis", *Int. J. Geosynthetics and Ground Eng.*, **10**(1), 6.

Daviran, M, Shamekhi, M., Ghezelbash, R. and Maghsoudi, A. (2023), "Landslide susceptibility prediction using artificial neural networks, SVMs and random forest: hyperparameters tuning by genetic optimization algorithm", *Int. J. Environ. Sci. Technol.*, **20**(1), 259-276. https://doi.org/10.1007/s13762-022-04491-3

Daviran, Mehrdad, Maghsoudi, A., Ghezelbash, R. and Pradhan, B. (2021), "A new strategy for spatial predictive mapping of mineral prospectivity: Automated hyperparameter tuning of random forest approach", *Comput. Geosci.*, **148**, 104688. https://doi.org/10.1016/j.cageo.2021.104688.

Dawei, Y., Bing, Z., Bingbing, G., Xibo, G. and Razzaghzadeh, B. (2023), "Predicting the CPT-based pile set-up parameters using HHO-RF and PSO-RF hybrid models", *Struct. Eng. Mech.*, **86**(5), 673-686. https://doi.org/10.12989/sem.2023.86.5.673.

Elias, V., Christopher, B. R., Berg, R.R. and Berg, R.R. (2001), "Mechanically stabilized earth walls and reinforced soil slopes: design and construction guidelines (updated version). United States. Federal Highway Administration.

Epstein, D., Badgley, J. and Calley, C. (2018), "*Geosynthetic reinforced soil–integrated bridge aystem evaluation*", United States. Federal Highway Administration. Office of Corporate Research.

Esmaeili-Falak, M. and Benemaran, R.S. (2024), "Ensemble extreme gradient boosting based models to predict the bearing capacity of micropile group", *Appl. Ocean Res.*, **151**, 104149. https://doi.org/10.1016/j.apor.2024.104149.

Fan, G.F., Zhang, L.Z., Yu, M., Hong, W.C. and Dong, S.Q. (2022), "Applications of random forest in multivariable response surface for short-term load forecasting", *Int. J. Elec. Power Energ. Syst.* **139**, 108073. https://doi.org/10.1016/j.ijepes.2022.10807.

Gueymard, C.A. (2014), "A review of validation methodologies and statistical performance indicators for modeled solar radiation data: Towards a better bankability of solar projects", *Renew. Sustain. Energy Rev.*, **39**, 1024-1034. https://doi.org/10.1016/j.rser.2014.07.117.

Hassankhani, E. and Esmaeili-Falak, M. (2024), "Soil–Structure interaction for buried conduits influenced by the coupled effect of the protective layer and trench installation", *J. Pipe. Syst. Eng. Pract*., **15**(2), 04024012. https://doi.org/10.1061/JPSEA2.PSENG-1547.

Hatami, K. and Bathurst, R.J. (2005), "Development and verification of a numerical model for the analysis of geosynthetic-reinforced soil segmental walls under working stress conditions", *Can. Geotech. J.*, **42**(4), 1066-1085. https://doi.org/10.1139/t05-040.

Hatami, K. and Bathurst, R.J. (2006), "Numerical model for reinforced soil segmental walls under surcharge loading", *J. Geotech. Geoenviron. Eng.*, **132**(6), 673-684. https://doi.org/10.1061/(ASCE)1090-0241(2006)132:6(673).

Islam, M.S., Awal, M.A., Laboni, J.N., Pinki, F.T., Karmokar, S., Mumenin, K.M., Al-Ahmadi, S., Rahman, M.A., Hossain, M.S., and Mirjalili, S. (2022), "HGSORF: Henry gas solubility optimization-based random forest for C-section prediction and XAI-based cause analysis", *Comput. Biol. Medicine*, **147**, 105671. https://doi.org/10.1016/j.compbiomed.2022.105671.

Javeed, A., Zhou, S., Yongjian, L., Qasim, I., Noor, A. and Nour, R. (2019), "An intelligent learning system based on random search algorithm and optimized random forest model for improved heart disease detection", *IEEE Access*, **7**, 180235-180243. https://doi.org/10.1109/ACCESS.2019.2952107.

Joo, C., Park, H., Lim, J., Cho, H. and Kim, J. (2022), "Development of physical property prediction models for polypropylene composites with optimizing random forest hyperparameters", *Int. J. Intell. Syst.*, **37**(6), 3625-3653. https://doi.org/10.1002/int.22700.

Kazimierowicz-Frankowska, K. (2018), "Deformations of reinforced-soil retaining walls", *Proceedings of the 11th International Conference on Geosynthetics*, Seoul, Korea, 16-21.

Liu, J., Jiang, Y., Zhang, Y. and Sakaguchi, O. (2021), "Influence of different combinations of measurement while drilling parameters by artificial neural network on estimation of tunnel support patterns", *Geomech. Eng.*, **25**(6), 439-453. https://doi.org/10.12989/gae.2021.25.6439.

Khishe, M. and Mosavi, M.R. (2020), "Chimp optimization algorithm", *Exp. Syst. Appl.*, **149**, 113338. https://doi.org/10.1016/j.eswa.2020.113338.

Khosrojerdi, M., Xiao, M., Qiu, T. and Nicks, J. (2017), "Evaluation of prediction methods for lateral deformation of GRS walls and abutments", *J. Geotech. Geoenviron. Eng.*, **143**(2), 6016022. https://doi.org/10.1061/(ASCE)GT.1943-5606.000159.

Khosrojerdi, M., Xiao, M., Qiu, T. and Nicks, J. (2020), "Prediction equations for estimating maximum lateral displacement and settlement of geosynthetic reinforced soil abutments. *Comput. Geotech.*, **125**, 103622. https://doi.org/10.1016/j.compgeo.2020.103622.

Lemonnier, P., Soubra, A.H. and Kastner, R. (1998), "Variational displacement method for geosynthetically reinforced slope stability analysis: I. Local stability", *Geotext. Geomembranes*, **16**(1), 1-25. https://doi.org/10.1016/S0266-1144(97)10020-6.

Leshchinsky, D., and Han, J. (2004), "Geosynthetic reinforced multitiered walls", *Journal of Geotechnical and Geoenvironmental Engineering*, **130**(12), 1225–1235. https://doi.org/10.1061/(ASCE)1090-0241(2004)130:12(1225)

Leshchinsky, D., Hu, Y. and Han, J. (2004), "Limited reinforced space in segmental retaining walls", *Geotext. Geomembranes*, **22**(6), 543-553. https://doi.org/10.1016/j.geotexmem.2004.04.002.

Liaw, A. and Wiener, M. (2002), "Classification and regression by random Forest", *R News*, **2**(3), 18-22.

Liu, H. (2012), "Long-term lateral displacement of geosynthetic-

reinforced soil segmental retaining walls", *Geotext. Geomembranes*, **32**, 18-27. https://doi.org/10.1016/j.geotexmem.2011.12.001

Mandal, J.N. and Jambale, K.S. (1992), "Analysis of a geosynthetic reinforced soil wall by the limit equilibrium method", *Constr. Build. Mater.*, **6**(3), 173-177. https://doi.org/10.1016/0950-0618(92)90012-N

Mirjalili, S. (2015), "The ant lion optimizer", *Advances in Engineering Software*, **83**, 80-98. https://doi.org/10.1016/j.advengsoft.2015.01.01.

Mirzaeiabdolyousefi, M., Mahmoodzadeh, A., Ibrahim, H.H., Rashidi, S., Majeed, M.K. and Mohammed, A.H. (2022), "Prediction of squeezing phenomenon in tunneling projects: Application of Gaussian process regression", *Geomech. Eng.*, **30**(1), 11–26. https://doi.org/10.12989/gae.2022.30.1.011.

Mo, J.Z., Zhou, S.L., He, G.C., Wang, C.Z. and Yang, C.Y. (2007), "Study on potential failure surface model of reinforced soil retaining walls", *J. China Railway Soc.*, **29**(6), 69-73.

Momeni, E., Yarivand, A., Dowlatshahi, M.B., and Armaghani, D.J. (2021), "An efficient optimal neural network based on gravitational search algorithm in predicting the deformation of geogrid-reinforced soil structures", *Transport. Geotech.*, **26**, 100446. https://doi.org/10.1016/j.trgeo.2020.100446.

Officials, T. (2009), "AASHTO LRFD bridge design guide specifications for GFRP-reinforced concrete bridge decks and traffic railings", AASHTO.

Ozturk, T. (2014), "Artificial neural networks approach for earthquake deformation determination of geosynthetic reinforced retaining walls", *Int. J. Intel. Syst. Appl. Eng.*, **2**(1), 1–9. https://doi.org/10.18201/ijisae.53315.

Pan, J.S., Zhang, L.G., Wang, R.B., Snášel, V. and Chu, S.C. (2022), "Gannet optimization algorithm: A new metaheuristic algorithm for solving engineering optimization problems", *Math. Comput. Simul.*, **202**, 343-373. https://doi.org/10.1016/j.matcom.2022.06.007

Probst, P., Wright, M.N. and Boulesteix, A. (2019), "Hyperparameters and tuning strategies for random forest", *Wiley Interdisciplinary Reviews: Data Mining and Knowledge Discovery*, **9**(3), e1301. https://doi.org/10.1002/widm.1301.

Qi, C., Chen, Q., Fourie, A. and Zhang, Q. (2018), "An intelligent modelling framework for mechanical properties of cemented paste backfill", *Minerals Eng.*, **123**, 16-27. https://doi.org/10.1016/j.mineng.2018.04.010

Rahmaninezhad, S.M. and Han, J. (2021), "Lateral facing deflections of geosynthetic-reinforced retaining walls under footing loading", *Transport. Geotech.*, **30**, 100594. https://doi.org/10.1016/j.trgeo.2021.100594.

Raja, M.N.A., Jaffar, S.T.A., Bardhan, A. and Shukla, S.K. (2022), "Predicting and validating the load-settlement behavior of large-scale geosynthetic-reinforced soil abutments using hybrid intelligent modeling", *J. Rock Mech. Geotech. Eng.*, https://doi.org/10.1016/j.jrmge.2022.04.012.

Raja, M.N.A. and Shukla, S.K. (2021), "Predicting the settlement of geosynthetic-reinforced soil foundations using evolutionary artificial intelligence technique", *Geotext. Geomembranes*, **49**(5), 1280=1293. https://doi.org/10.1016/j.geotexmem.2021.04.007.

Rowe, R.K. and Ho, S.K. (1998), "Horizontal deformation in reinforced soil walls", *Can. Geotech. J.*, **35**(2), 312-327. https://doi.org/10.1139/t97-062.

Stuedlein, A.W., Bailey, M., Lindquist, D., Sankey, J. and Neely, W.J. (2010), "Design and performance of a 46-m-high MSE wall", *J. Geotech. Geoenviron. Eng.*, **136**(6), 786-796. https://doi.org/10.1061/(ASCE)GT.1943-5606.0000294.

Sun, D., Wen, H., Wang, D. and Xu, J. (2020), "A random forest model of landslide susceptibility mapping based on hyperparameter optimization using Bayes algorithm", *Geomorphology*, **362**, 107201. https://doi.org/10.1016/j.geomorph.2020.107201.

Sun, D., Xu, J., Wen, H. and Wang, D. (2021), "Assessment of landslide susceptibility mapping based on Bayesian hyperparameter optimization: A *comparison* between logistic regression and random forest", *Eng. Geol.*, **281**, 105972. https://doi.org/10.1016/j.enggeo.2020.10597.

Wang, S., Zhuang, J., Zheng, J., Fan, H., Kong, J. and Zhan, J. (2021), "Application of Bayesian hyperparameter optimized random forest and XGBoost model for landslide susceptibility mapping", *Front. Earth Sci.*, **9**, 712240. https://doi.org/10.3389/feart.2021.712240.

Wu, J. and Pham, T. (2010), "An analytical model for calculating lateral movement of a geosynthetic-reinforced soil (GRS) wall with modular block facing", *Int. J. Geotech. Eng.*, **4**(4), 527-535. https://doi.org/10.3328/IJGE.2010.04.04.527-535.

Wu, J.T.H., Lee, K.Z.Z. and Pham, T. (2006), "Allowable bearing pressures of bridge sills on GRS abutments with flexible facing", *J. Geotech. Geoenviron. Eng.*, **132**(7), 830-841. https://doi.org/10.1061/(ASCE)1090-0241(2006)132:7(830).

Xu, C., Gordan, B., Koopialipoor, M., Armaghani, D.J., Tahir, M. M. and Zhang, X. (2019), "Improving performance of retaining walls under dynamic conditions developing an optimized ANN based on ant colony optimization technique", *IEEE Access*, **7**, 94692–94700. https://doi.org/10.1109/ACCESS.2019.2927632.

Yang, G.Q., Xu, C. and Zhang, M.X. (2016), "Geosynthetics reinforcement soil structure application guidance", Beijing: China Communications Press.

Yaychi, B.M. and Esmaeili-Falak, M. (2024), "Estimating axial bearing capacity of driven piles using tuned random forest frameworks", *Geotech. Geol. Eng.*, **42**(8), 7813-7834. https://doi.org/10.1007/s10706-024-02952-9.

Yoo, C. and Jung, H.S. (2004), "Measured behavior of a geosynthetic-reinforced segmental retaining wall in a tiered configuration", *Geotext. Geomembranes*, **22**(5), 359-376. https://doi.org/10.1016/S0266-1144(03)00064-5.

Yoo, C. and Kim, S.B. (2008), "Performance of a two-tier geosynthetic reinforced segmental retaining wall under a surcharge load: Full-scale load test and 3D finite element analysis", *Geotext. Geomembranes*, **26**(6), 460–472. https://doi.org/10.1016/j.geotexmem.2008.05.008

Zhang, K., Zhang, Y. and Razzaghzadeh, B. (2024), "Application of the optimal fuzzy-based system on bearing capacity of concrete pile", *Steel Compos. Struct.*, **51**(1), 25-41. https://doi.org/10.12989/scs.2024.51.1.025.

GC